IEEE Access
Multidisciplinary | Rapid Review | Open Access Journal

Received February 21, 2019, accepted February 25, 2019, date of publication March 5, 2019, date of current version March 25, 2019.

Digital Object Identifier 10.1109/ACCESS.2019.2902851

ISVD-Based In-Band Noise Reduction Approach Combined With Envelope Order Analysis for Rolling Bearing Vibration Monitoring Under Varying Speed Conditions

YONG REN, WEI LI, ZHENCAI ZHU, AND FAN JIANG
School of Mechanical and Electrical Engineering, China University of Mining and Technology, Xuzhou 221116, China

Corresponding author: Wei Li (liwei_cmee@163.com)

This work was supported in part by the National Natural Science Foundation of China under Grant 51475455 and Grant 51605478, in part by the Natural Science Foundation of Jiangsu Province under Grant BK20160276 and Grant BK20160251, in part by the China Postdoctoral Science Foundation under Grant 2017M621862, and in part by the Project Funded by the Priority Academic Program Development of Jiangsu Higher Education Institutions (PAPD).

ABSTRACT In practical applications, the signal measured from a complex mechanical system is usually disturbed by various noises due to the compounded effect of interferences of other machine elements and background noises, especially under varying speed conditions. Resonance-based approaches have been proven to be effective methods to address this problem. However, even if the optimal resonance band is accurately determined, the in-band noise with frequency content in the range covered by the band-pass filter is not eliminated. To avoid missed diagnosis and misdiagnosis of faults in bearings, an iterated SVD (ISVD)-based in-band noise reduction method combined with envelope order spectrum analysis is proposed in this paper. First, the optimal frequency band of a vibrational signal is determined with the help of an enhanced wavelet packet transform kurtogram, in which the kurtosis of each node is calculated based on the envelope spectrum of a signal be reconstructed using the wavelet packet coefficients. The node with the maximum kurtosis value is used to reconstruct the signal. Second, the envelope of a reconstructed signal is calculated by Hilbert transform and the ISVD method is applied to it to reduce the in-band noise. To avoid the destruction of useful information caused by excessive iteration, a threshold is set to determine the number of iterations. After iterative processing, a de-noised signal is reconstructed based on the relationship between the singular value and a frequency component. Finally, the reconstructed signal is resampled and transformed into the fault characteristic order domain where the bearing fault type can be identified from the envelope order spectra. The simulations and experiments were used to validate the efficacy of the proposed method. Compared with the spectral subtraction method, the ISVD method can suppress in-band noise efficiently and beneficial to extract the fault characteristic order under variable speed conditions.

INDEX TERMS Rolling bearing, wavelet package transform kurtogram, iterated SVD, FCO, variable speed.

I. INTRODUCTION

Rolling bearings are one of the most commonly used support elements in rotation machinery, and their failure may lead to fatal equipment breakdown and significant economic losses. Once a local bearing defect is developed, contact of such defects with mating surfaces generates a series of impulses, which usually carry rich information about their health condition [1]–[2]. Thus, it is crucial to effectively extract these features from the vibration signals for successful rolling bearing fault diagnosis. However, rolling bearings often work under variable speed conditions in practice, which will causes frequency spectrum smearing, and the fault feature components will no longer be observable and detected as discrete frequency lines. In addition, background noise and vibration interferences from other components can severely obscure the fault impulses, especially when the vibration sensor cannot be mounted in the near vicinity of the bearing being

The associate editor coordinating the review of this manuscript and approving it for publication was Zhixiong Peter Li.

monitored [3]. Therefore, how to effectively extract fault features from background noise under varying speed conditions has attracted much attention.

During the past few years, many techniques have been proposed to solve this problem [4]–[6]. Among these methods, the resonance demodulation technique (RDT) is regarded as an effective tool [7]–[8]. Considering that the fault impulse has a wide frequency band and usually excites resonances in the system at a much higher frequency, the signal-to-noise ratio (SNR) is higher and the vibration features can be demodulated in a suitable frequency band [9]–[10]. The major challenge in the application of the RDT lies in how to determine the optimal frequency band for demodulation. To accurately determine the high frequency resonance band, spectral kurtosis (SK) was proposed by Zhao *et al.* [11], which has been indicated to be an effective index for the identification of the response of the system. Inspired by this development, Antoni proposed the fast kurtogram (FK) based on the short-time Fourier transform (STFT) [12]. Many methods have been proposed to further enhance the accuracy of the FK for discovering the sensitive frequency band [13]. In [14], Lei *et al.* found that a wavelet packet transform (WPT) can generate more precise filters than a STFT-based method. Therefore, they suggested a WPT to be used to construct a kurtogram (WPTK), and the transients hidden in a noisy signal can be filtered by this method. To extract transient impulsive signals under a low SNR condition, an enhanced WPTK is constructed by replacing the kurtosis of the temporal signals extracted from wavelet packet nodes with the power spectrum kurtosis in [8]. Although the optimal frequency band is extracted effectively, only the noise outside the selected frequency band is removed, the in-band noise with frequency content in the band is not eliminated. If the strength of such a noise is high, it still remains a challenging task to extract fault features from the filtered non-stationary vibration signals. Therefore, the filtered signal needs to be further processed.

Many in-band de-noising methods have been proposed in recent decades. In [15], Bozchalooi *et al.* use a spectral subtraction to trim down the in-band noise. It is assumed that the energy of the background noise is uniformly distributed over a narrow band, and based on this assumption, they applied the smoothness minimization criterion to find the proper subtraction value to enhance the hidden impulses. In [16], an impulse reconstruction scheme based on an improved harmonic product spectrum and sideband product spectrum is proposed to reduce the in-band noise. In [17], an energy kurtosis demodulation (EKD) technique is introduced by Wang et al. and the SNR is enhanced by the use of a maximum kurtosis deconvolution filter. As a data-driven signal processing method, the SVD based de-noising approach is essentially energy-based, and tends to highlight the high-energy regular components in the measured signal [18], and compared with other signal processing methods, it is faster and easier to implement. As mentioned in [19], the effect of signal SVD-based de-noising is mainly affected by two aspects: (1) the structure of the matrix to be analysed. In practice, the measured signals are always expressed as time series rather than matrices. Therefore, many methods have been proposed for reshaping the time series into a matrix as a preparation for SVD. Unfortunately, there is no single indicator of how to construct a matrix properly, and studies often adopt different matrix types to solve different problems [20], including the Toeplitz matrix [21], cycle matrix [22] and Hankel matrix [23]; (2) the identification of valid singular values. The core of SVD-based de-noising is how to choose the effective singular value to reconstruct the signal [19]. To solve this problem, a difference spectrum algorithm and a correlation coefficient-based selection algorithm were introduced to select the effective singular values [24]. In summary, the available SVD-based de-noising methods are based on constructing the signal matrix properly and selecting the singular values effectively. However, the frequency spectrum of the filtered signal is smeared due to the varying speed conditions, which increases the difficulty of extracting effective singular values [25]. To extract the fault characteristics exactly, the order tracking (OT) method has been successfully used to eliminate the influence of varying speed by resampling the non-stationary time signal into the stationary signal in the angular domain [26]. The fault impulses are rearranged to be equal in the angular domain, and the fault style can be identified strictly because the fault features are arranged into discrete order lines in the Fourier transform.

Considering the above, an iterated SVD (ISVD)-based in-band noise reduction method combined with an enhanced WPTK and OT is proposed in this paper to extract fault information accurately. Firstly, the optimal frequency band of a vibrational signal is determined with the help of an enhanced wavelet packet transform kurtogram (WPTK), in which the kurtosis of each node is calculated based on the envelope spectrum of a signal be reconstructed using the wavelet packet coefficient. The node with the maximum kurtosis value is used to reconstruct the signal. Secondly, the ISVD is applied to the envelope of the reconstructed signal to reduce the in-band noise, the transient fault impulse components in the signal is enhanced based on the relationship between the singular value and a frequency component. Finally, the reconstructed signal is resampled and transformed into the fault characteristic order (FCO) domain where the bearing fault type can be identified from the envelope order spectra.

The remainder of this paper is arranged as follows. Section 2 introduces an analytical model to describe the collected vibration signal and analyzes the distribution character of a different component. Based on the theoretical analysis, the theory of ISVD is proposed in Section 3. Simulation and experiment studies are discussed in Sections 4 and 5, respectively. Conclusions are drawn in Section 6.

II. THE DISTRUCTION CHARACTER OF THE MULTI-COMPONENT SIGNAL ENVELOPE

A. ANALYTICAL MODEL FOR DIFFERENT COMPONENTS

Considering a real situation from industry, the collected vibration signal is usually composed of many components when faults occur in a rotating machinery system, and it is not accessible or is difficult to inspect directly, especially in the early stages of failure. This paper mainly focus on early fault diagnosis of rolling bearing in varying speed conditions, the collected vibration signal contains deterministic and random components, the former caused by factors such as misalignment of the rotor or gear meshing, and the latter induced by the bearing faults. The signal of a system can be written as:

$$X(t) = D(t) + R(t) + n(t) \tag{1}$$

where $X(t)$ is the collected vibration signal, $D(t)$ represents the deterministic component, $R(t)$ denotes the random component, and $n(t)$ is Gaussian noise.

The deterministic component $D(t)$ is given by

$$D(t) = \sum_{b=1}^{B} A_{b,D} \cos(2\pi f_{b,D} f_r(t) t + \phi_{b,D}) \tag{2}$$

The model of cycle impulse responses representing the faulty bearing part $R(t)$ is given by

$$R(t) = \sum_{m=1}^{M} A_{m,R} \times \exp(-\beta(t - T_{m,R})) \cos(2\pi f_{b,R}(t - T_{m,R}) + \phi_{m,R}) \tag{3}$$

The noise $n(t)$ can be written as:

$$n(t) = awgn(X(t), P) \tag{4}$$

where A is the amplitude, f_b is the corresponding base frequency, f_r is the time-varying speed, ϕ_m is the initial phase, β represents the structural damping coefficient, and T_m is the occurrence time of the m th impulse. It is worth noting that $\{T_m, m = 1, 2, 3, \ldots, M\}$ is an independent increment process due to the varying rotating speed; the randomicity of the process is increased as the rolling elements experience some random slippages, which are caused by the changing of loads and can be described as $\{\xi | \xi_m = \mu(T_m - T_{m-1}), \mu = 0.01 \sim 0.02, m = 2, 3, 4, \ldots\}$. $awgn$ is a function of MATLAB that is used to generate white Gaussian noise. P specifies SNR.

B. THE RULE OF THE MULTI-COMPONENT SIGNAL ENVELOPE

To obtain the energy change caused by the bearing fault, the envelope signal of the collected signal is calculated here. As mentioned in [27], the energy of white noise is uniformly distributed along the frequency. Therefore, to reduce the difficulty of analysis, the noise can be neglected here. Then, the analytical form of the signal can be written as:

$$Y(t) = X(t) + j\widehat{X}(t) \tag{5}$$

where $\hat{X}(t)$ is the Hilbert transform of $X(t)$. Then, the squared envelope of the signal is given by

$$\begin{aligned} |Y(t)|^2 &= X(t)^2 + \widehat{X}(t)^2 \\ &= [D(t) + R(t)]^2 + [\widehat{D}(t) + \widehat{R}(t)]^2 \\ &= D(t)^2 + R(t)^2 + 2D(t)R(t) + \widehat{D}(t)^2 + \widehat{R}(t)^2 + 2\widehat{D}(t)\widehat{R}(t) \end{aligned} \tag{6}$$

where $\hat{D}(t)$ and $\hat{R}(t)$ are the Hilbert transforms of $D(t)$ and $R(t)$, respectively. It is clear that the squared envelope of the useful signal also includes the cross-terms of these two kinds of signals and their Hilbert transforms. Generally, the unit impulse response function is the product of a high-frequency oscillation component and a single side exponential damping function [28]. When the unit impulse response function satisfies the Bedrosian theorem, the Hilbert transforms of $D(t)$ and $R(t)$ can be written as:

$$\begin{cases} \widehat{D}(t) = H\{D(t)\} = D(t) * \frac{1}{\pi t} = \sum_{b=1}^{B} A_b \sin(2\pi f_b f_r(t) t + \varphi_l) \\ \widehat{R}(t) = H(R(t)) = R(t) * \frac{1}{\pi t} \\ = -\sum_{m=1}^{M} A_{bear,m} \\ \qquad \exp(-\beta(t - T_m)) \sin(2\pi f_{bear}(t - T_m) + \phi_m) \end{cases} \tag{7}$$

where H{•} denotes the Hilbert transform operator and $*$ denotes the convolution operator. In practice, the number of deterministic components is always smaller than that of the fault impulses, i.e. $B \ll M$. Thus, the squared envelope of the signal can be developed as: Thanks to the slow time-variability of the amplitude of the deterministic component, the first part of Eq. (8), as shown at the top of the next page, can be seen as the trend term of the envelope signal. The second part carries the main fault information that contains the energies and moments of the impulse occurrence, which are crucial for the bearing fault diagnosis. In contrast to the part mentioned above, the next parts combined with the deterministic component and random impulse responses together, and the latter is modulated by the former. What is worse, the carrier frequencies of these impulse responses change with the varying frequency of the deterministic component, which leads to spectrum complexity. In addition, the latter two parts contain impulse responses that have a wide frequency band, and some resonant frequencies of the system can also be excited. Therefore, the fault features modulated by the resonant frequencies are still complex unlike those of the constant speed condition, and the fault features are no longer discrete frequency lines in their envelope spectrum.

III. THE PROPOSED BEARING FAULT DIAGNOSIS METHOD

A. WAVELET PACKET TRANSFORM KURTOGRAM

Rolling bearing local defects always result in a series of impulses, thus exciting resonances and leading to modulations on resonances. Therefore, much valuable fault

$$
\begin{aligned}
|Y(t)|^2 &= D(t)^2 + R(t)^2 + 2D(t)R(t) + \widehat{D}(t)^2 + \widehat{R}(t)^2 + 2\widehat{D}(t)\widehat{R}(t) \\
&= (\sum_{b=1}^{B} A_b \cos(2\pi f_b f_r(t)t + \varphi_l))^2 + (-\sum_{m=1}^{M} A_{bear,m} \exp(-\beta(t - T_m)) \cos(2\pi f_{bear}(t - T_m) + \phi_m))^2 \\
&\quad + 2\sum_{b=1}^{B} A_b \cos(2\pi f_b f_r(t)t + \varphi_l) \sum_{m=1}^{M} A_{bear,m} \exp(-\beta(t - T_m)) \cos(2\pi f_{bear}(t - T_m) + \phi_m) \\
&\quad + (\sum_{b=1}^{B} A_b \sin(2\pi f_b f_r(t)t + \varphi_l))^2 + (\sum_{m=1}^{M} A_{bear,m} \exp(-\beta(t - T_m)) \sin(2\pi f_{bear}(t - T_m) + \phi_m))^2 \\
&\quad - 2\sum_{b=1}^{B} A_b \sin(2\pi f_b f_r(t)t + \varphi_l) \sum_{m=1}^{M} A_{bear,m} \exp(-\beta(t - T_m)) \sin(2\pi f_{bear}(t - T_m) + \phi_m) \\
&= \sum_{b=1}^{B} A_b^2 + \sum_{m=1}^{M} A_{bear,m}^2 \exp(-2\beta(t - T_m)) \\
&\quad + 2\sum_{b,m=1}^{B} A_b A_{bear,m} \exp(-\beta(t - T_m)) \cos(2\pi(f_b f_r(t)t + f_{bear}(t - T_m) + \varphi_l + \phi_m) \\
&\quad + 2\{\sum_{b=1}^{B} A_b \cos(2\pi f_b f_r(t)t + \varphi_l) \sum_{m=B+1}^{M} A_{bear,m} \exp(-\beta(t - T_m)) \cos(2\pi f_{bear}(t - T_m) + \phi_m) \\
&\quad - \sum_{b=1}^{B} A_b \sin(2\pi f_b f_r(t)t + \varphi_l) \sum_{m=B+1}^{M} A_{bear,m} \exp(-\beta(t - T_m)) \sin(2\pi f_{bear}(t - T_m) + \phi_m)\}
\end{aligned} \tag{8}
$$

information is contained in the resonance frequency band. Lots of methods have been proposed to select the frequency band, among which, the kurtosis based method is one of the most powerful techniques [29]. The wavelet packet transform kurtogram (WPTK) is used in this paper due to its filters precisely and match the fault characteristics of noisy signals exactly.

A wavelet packet transform (WPT) is a generalized case of an orthogonal wavelet transform (WT) [30]. Different from a WT, a WPT not only decomposes the low-frequency band into a lower resolution space but also processes the high-frequency band further by using wavelet bases. Thus, a more precise frequency band over the whole analysed frequency band can be obtained. As a multi-resolution analysis method, a WPT can be implemented based on wavelet filters and the decomposition signal at different depths can be calculated as follows [8], [14]:

$$
\begin{cases}
x_j^i = \sqrt{2} \sum_{n=0}^{K} h(n) x_{j+n}^{i-1} \\
x_{j+1}^i = \sqrt{2} \sum_{n=0}^{K} g(n) x_{j+n}^{i-1}
\end{cases} \tag{9}
$$

where i is the number of decomposition levels; j denotes the number of decomposed frequency band signals, where $j = 1, 2, \cdots, 2^i - 1, 2^i$; x_j^i is the j th decomposed frequency band signal at level i; $h(n)$ and $g(n)$ are a pair of conjugate mirror filters based on wavelets.

In a WPT, the recursive splitting of a signal can be represented in a binary tree, which is named the wavelet packet tree. Each node of such a tree corresponds to a frequency band signal that has the same length as the original signal. However, the order of the frequency bands in the tree is disordered [31]. In order to analyze conveniently, these nodes need to be rearranged in accordance with the frequency from low to high. The kurtosis of the temporal signal extracted from wavelet packet nodes is used to locate the optimal frequency band [14]. However, it will fails under strong noise disturbance, especially with an impulsive noise. To reduce the impact of impulse noise, the kurtosis of each node is calculated based on the envelope spectrum of a signal be reconstructed using the wavelet packet coefficients. Replacing it with the original kurtosis, an enhanced WPTK is constructed.

The envelope spectrum kurtosis is calculated for each reconstructed signal and can be expressed as follows:

$$
K_j^i = \frac{\sum_{n=1}^{N} (X_j^i(n) - \bar{X}_j^i)^4}{(N-1)\sigma_{X_j^i}^4} \tag{10}
$$

where i represents the i th layer of wavelet packet decomposition; j is the j th node in the i th layer; x_j^i is the original signal; X_j^i is the envelope spectrum; $\bar{X}_j^i$, $\sigma_{X_j^i}$ and N are the mean value, the standard deviation and the length of the signal corresponding to the reconstructed signal, respectively, and

K_j^i is the envelope spectrum kurtosis.

$$[i, j] = \arg\max(K_j^i) \tag{11}$$

Similar to the original kurtogram, the node with the maximum envelope spectrum kurtosis is selected by equation (11) and the corresponding frequency band is the optimal frequency band.

B. ISVD-BASED IN-BAND DE-NOISING METHOD

1) THE RULE OF SINGULAR VALUES DISTRIBUTION

Singular value decomposition (SVD) is an effective nonlinear and non-stationary signal processing method, and its application in de-noising has been proven to be efficient [32]. In [20], only two consecutive non-zero singular values are always generated for one frequency component signal. For an array $Y(t)$ that contains only one frequency component and has length N, the SVD of it can be denoted as:

$$\begin{aligned} SVD(H(Y(t))) &= SVD\left(\begin{bmatrix} Y_{t_1} & Y_{t_2} & \cdots & Y_{t_n} \\ Y_{t_2} & Y_{t_3} & \cdots & Y_{t_{n+1}} \\ \vdots & \vdots & \cdots & \vdots \\ Y_{t_m} & Y_{t_{m+1}} & \cdots & Y_{t_N} \end{bmatrix}\right) \\ &= U_H(\sigma_1, \sigma_2, O)V_H^T \end{aligned} \tag{12}$$

where O represents a zero matrix, $U_H = (u_1, u_2, \cdots, u_m)$ and $V_H = (v_1, v_2, \cdots, v_m)$. Thus, $H(Y(t)) = u_1\sigma_1 v_1^T + u_2\sigma_2 v_2^T$. Therefore,

$$\begin{aligned} |H(Y(t))|^2 &= \left|u_1\sigma_1 v_1^T + u_2\sigma_2 v_2^T\right|^2 \\ &= \sigma_1^2 \sum_{i=1}^{\infty/2} u_{1,i}^2 \sum_{i=1}^{\infty/2} v_{1,i}^2 + \sigma_2^2 \sum_{i=1}^{\infty/2} u_{2,i}^2 \sum_{i=1}^{\infty/2} v_{2,i}^2 \\ &\quad + 2\sigma_1\sigma_2 \sum_{i=1}^{\infty/2} u_{1,i}u_{2,i} \sum_{i=1}^{\infty/2} v_{1,i}v_{2,i} \\ &= \sigma_1^2 + \sigma_2^2 \end{aligned} \tag{13}$$

As a result, the sum of the square of the singular values is proportional to the energy of the corresponding instantaneous frequency signal. After the different components of the signal are arranged in descending order of energy, the singular values of each component can be determined by analysing the energy of that component, e.g., the singular values of the i th energy component are σ_{2i-1} and σ_{2i}. From the above mentioned results, it can be concluded that the signal to be analysed should satisfy the following three conditions to separate the effective component:

1) the signal contains a finite frequency component: $1 \leq f_{numb} \ll +\infty$;
2) the energy of each frequency component is different from that of each other: $E_{f_{numb,i}} \neq E_{f_{numb,j}}$;
3) the signal to be analysed is long enough: $N \geq 4 \times f_{numb} \pm (0, 2) - 1$ (see Appendix).

However, in the case of a continuous increase in speed, the frequency of the signal is time-varying; in other words, the number of instantaneous frequency components contained in the signal increases with the length of the signal, so conditions a) and c) cannot be satisfied at the same time. In addition, from the view of statistical analysis, the amplitude of white noise satisfies the normal distribution, and the frequency energy is evenly distributed, while in practice, the length of the signal to be analysed is limited, the white noise may not always have statistical properties, and there is no guarantee that condition b) will be established at any time. Therefore, the SVD of the signal matrix in the time domain cannot accurately extract the useful information of the signal under varying speed conditions.

2) ISVD METHOD

It can be seen from the previous analysis that under variable speed conditions, the signal frequency components are time-varying. The analysis of the signal with the same resolution cannot obtain effective analysis results. To solve this problem, S.Mallat proposed the concept of multi-resolution analysis in the construction of orthogonal wavelets in 1988. Zhao *et al.* [20] proposed a new Hankel matrix construction method combined with iterative analysis to introduce the idea of multi-resolution into SVD, which has been successfully applied under constant speed conditions. However, for non-stationary signals, especially if the effective low-frequency components of the signal are modulated into high frequency, the fault information of the signal is lost by the discarding of detailed components. To solve this problem, an iterated SVD is proposed here.

A new Hankel matrix is constructed by using a raw signal $X_i = [x_1, x_2, x_3, \cdots, x_{n-2}, x_{n-1}, x_n]$, $n \in N+$, and given as:

$$\mathrm{H}(X_i) = \begin{bmatrix} x_1, x_2, x_3, \cdots, x_{n-3}, x_{n-2}, x_{n-1} \\ x_2, x_3, x_4, \cdots, x_{n-2}, x_{n-1}, x_n \end{bmatrix}.$$

then,

$$\begin{aligned} SVD(H(X_i)) &= SVD\left(\begin{bmatrix} x_1, x_2, x_3, \cdots, x_{n-3}, x_{n-2}, x_{n-1} \\ x_2, x_3, x_4, \cdots, x_{n-2}, x_{n-1}, x_n \end{bmatrix}\right) \\ &= U_i(\sigma_{i1}, \sigma_{i2})V_i^T \end{aligned} \tag{14}$$

where, $U_i = (u_{i1}, u_{i2})$, $U_i \in R^{2\times 2}$, $V_i = (v_{i1}, v_{i2}, \cdots, v_{i(n-2)}, v_{i(n-1)})$, $V_i \in R^{(n-1)\times 2}$, σ_i is the matrix singular value and $\sigma_{i1} \geq \sigma_{i2} \geq 0$; then, the Hankel matrix $H(X_i) = A_i + D_i = u_{i1}\sigma_{i1}v_{i1}^T + u_{i2}\sigma_{i2}v_{i2}^T$. Taking A_i as an example, and the corresponding reconstructed signal can be denoted as:

$$\begin{aligned} A_i = [&u_{i1,1}\sigma_{i1}v_{i1,1}, (u_{i1,1}\sigma_{i1}v_{i1,2} + u_{i1,2}\sigma_{i1}v_{i1,1})/2 \cdots, \\ &(u_{i1,1}\sigma_{i1}v_{i1,n-1} + u_{i1,2}\sigma_{i1}v_{i1,n-2})/2, u_{i1,2}\sigma_{i1}v_{i1,n-1}]. \end{aligned}$$

The same can be performed for D_i, and the corresponding reconstructed signal is denoted as:

$$\begin{aligned} D_i = [&u_{i2,1}\sigma_{i2}v_{i2,1}, (u_{i2,1}\sigma_{i2}v_{i2,2} + u_{i2,2}\sigma_{i2}v_{i2,1})/2, \cdots, \\ &(u_{i2,1}\sigma_{i2}v_{i2,n-1} + u_{i2,2}\sigma_{i2}v_{i2,n-2})/2, u_{i2,2}\sigma_{i2}v_{i2,n-1}]. \end{aligned}$$

It is worth noting that the envelope of the impulse response is concentrated at the low frequency band and has better aggregation [28]. Firstly, the signal envelope is calculated

with the Hilbert transform, and the trend term of the envelope signal is eliminated by a high-pass filter whose cutoff frequency is slightly higher than the minimum of the rotating frequency. Secondly, the 2-D Hankel matrix is constructed with the filtering signal, and after this matrix is decomposed by SVD, only two singular values can be got, the first one will be larger than the second one, each singular value and corresponding singular vector are used to reconstruct the signal, thus only two component signals can be got since each singular value is associated with a component signal. Calculate the root mean square error (RMSE) between the reconstructed signal corresponding to the larger singular value and the original signal, if the RMSE is below a preset threshold, then replace the original signal with the reconstructed signal and repeat the above steps until the RMSE is below the threshold. To improve the analysis efficiency, the correlation of different reconstructed components is calculated, and the components whose cross-correlation coefficient (CCO) is above a preset threshold are put together. When the RMSE between the adjacent envelopes satisfies the condition, calculate the SK of each reconstructed signal in the last layer and the one with the maximum SK value is used to replace the original signal. The SK is calculated as mentioned in [8]. The proposed procedure is shown in Fig. 1.

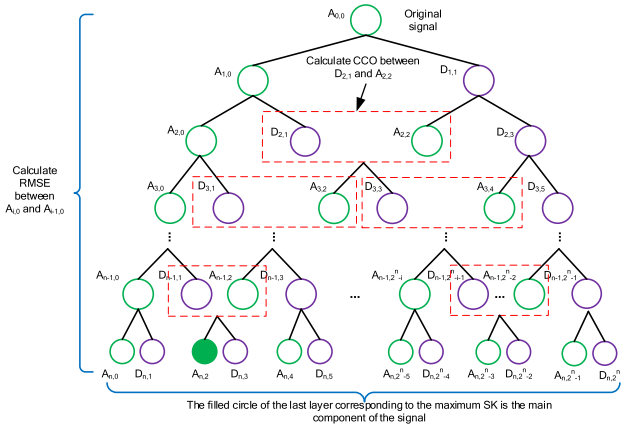

FIGURE 1. Flow chart of the proposed ISVD method.

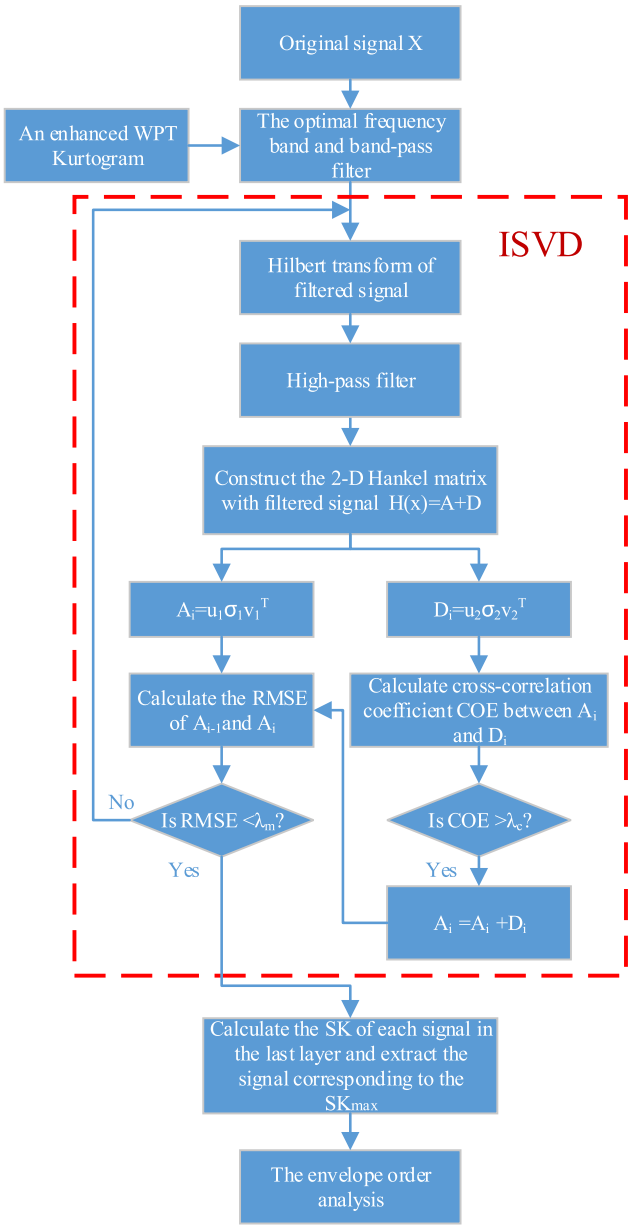

FIGURE 2. Schematic diagram of the proposed method.

C. SUMMARY OF THE PROPOSED METHOD

With the main steps described above, the schematic of the proposed method is shown in Fig. 2 and can be summarized as follows:

1) Extract the sensitive frequency band from the original signal X with the help of an enhanced WPTK and reconstruct the signal with the wavelet packet coefficient corresponding to the maximum envelope spectrum kurtosis;
2) Calculate the envelope of the reconstructed signal by the Hilbert transform;
3) Eliminate the trend term of the envelope signal by a low pass filter whose cutoff frequency is lower than the minimum of the rotating frequency.
4) Construct the 2-D Hankel matrix with the filtered envelope signal;
5) Reconstruct each part of the signal with different singular values and calculate the CCO; if CCO $>$ λ c add these parts together;
6) Calculate the RMSE between the adjacent layers with the first envelope signal; if RMSE $>$ λ m, turn back to step (2). Otherwise, continue with the steps below;
7) Calculate the SK of each component in the last layer and the signal corresponding to the maximum SK is used to replace the original signal;
8) The order analysis: resample the reconstructed signal into the angle domain and transform it into the fault characteristic order (FCO) domain. The relative

envelope order spectra can be calculated by the following formula:

$$A_{r,i} = \frac{A_i}{sum(\sum_{i=1}^{N} A_i)} \tag{15}$$

where A_i is the amplitude of the order spectrum and N is the length of the spectrum.

IV. SIMULATION ANALYSIS

As mentioned in Section 2, a synthetic signal $X(t)$ is constructed to simulate the rotor-bearing-gear system, and the simulation signal parameters in the model are given in Table 1.

TABLE 1. Parameters of the simulation model.

Length (N)	Speed (f_r/Hz)	Bearing resonance frequency (f_{bear}/kHz)	Sample rate (f_s/kHz)	Bearing amplitude coefficient ($A_{m,R}$)	Amplitude coefficient ($A_{b,D}$)
2^15	20-33	6	20	2	A_1=0.5, A_2=0.3 A_3=
SNR (P/dB)	Bearing FCO	Rotor FCO	Number of teeth (Z)	Slippage coefficient (ζ)	Damping characteristic (β)
-10	3.5	1	18	0.01	1200

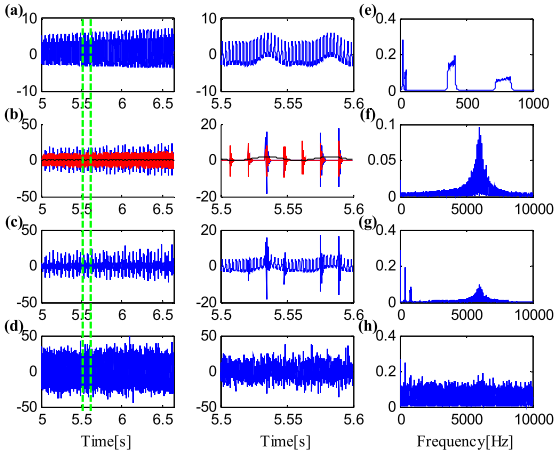

FIGURE 3. The simulation signal: (a) deterministic component, (b) random fault component (the red line is the fault pulse signal, and the black line is the frequency modulated signal), (c) mixed signal without noise, (d) noise-added mixed signal with SNR = -10dB, (e)-(h) FFT of different components, and the middle column is images locally enlarged in a range between the two green dotted lines.

In order to determine the type of fault exactly, the fault components should be extracted from the signal as accurately as possible. Therefore, the effectiveness of the deterministic components and noise interference need to be eliminated. In Figs. 3 (e) to (h), the Fast Fourier Transform (FFT) analysis of each component produces false frequency information due to the variable speed, but it still can observed that the difference in energy distribution between each component of the signal. The analysis results are illustrated in Fig. 4. Based on the speed information, the original simulation signal envelope is resampled into the angle domain directly to eliminate the influence from varying speed and the envelope order analysis result are shown in Figs. 4 (a) to (d), respectively. In Fig. 4 (d), only the second FCO can be observed. To reduce the influence of interferences, the WPTK of the signal is calculated as shown in Fig. 4 (e), in which the node with the maximum envelope spectrum kurtosis is selected and the corresponding frequency band is the optimal frequency band. In Fig. 4 (e), the maximum kurtosis is calculated at the 4th decomposition level, and its corresponding frequency band is [5625, 6250] Hz. The signal is reconstructed with the wavelet coefficient in this node, which is shown in Fig. 4 (f). Then, the envelope of the reconstructed signal is calculated by Hilbert transform as shown in Fig. 4 (g). The envelope is resampled into the angle domain. The angle domain signal and relative envelope order spectra analysis result are shown in Figs. 4 (h) and (i), respectively. It is clear that only first two FCOs can be found in Fig. 4 (i). However, it is often desirable to detect up to the third harmonic of the bearing defect frequency in the envelope spectrum [33], which means the reconstructed signal needs to be further processed. To further improve the SNR, the reconstructed signal is decomposed by ISVD, in which the prior threshold of the RMSE between the adjacent envelopes is set to 0.1, i.e., $\lambda_m = 0.1$, and the cross-correlation coefficient is set to 0.99, i.e., $\lambda_c = 0.99$. The cutoff frequency of the high-pass filter used for trend term elimination is set to 20 Hz, which is the minimum speed value. The reconstructed signal is de-noised, as shown in Fig. 4 (j). Its angle domain signal and the relative envelope order spectra analysis result are shown in Figs. 4 (k) and (l), respectively. The FCO and its first four fault orders can be easily identified in Fig. 4 (l). To show the effectiveness of the proposed method intuitively, time domain signal envelope at different time periods are shown in Fig. 5. Compared with Figs. 5 (b) and (c), although the amplitude of the signal decreases, the relative amplitude of shock signal component is more obvious in Fig. 5(d). Therefore, the proposed ISVD method may also reduce the intensity of frequency components other than the white noise, it helps the hidden impulses to manifest in the final de-noised signal, which is the main goal of this algorithm. To be more persuasive, the spectral subtraction method proposed by Bozchalooi *et al.* [15] is applied to these simulations, and the analysis results are shown in Fig. 6. Compared Fig. 4 (k) with Fig. 6 (a), the amplitude of shock signal component contained in the resampling signal obtained by ISVD is more obvious. Although the first three fault orders can be found in Fig. 6 (b), the relative envelope order spectra amplitudes corresponding to the first two FCO spectrum are smaller. In order to show the advantages of the proposed method intuitively, the amplitudes of the first four fault orders obtained by different ways are compared in Table 2.

From Table 2, it is clear that the method proposed in this paper can improve the SNR effectively. To further demonstrate the advantages of the proposed method, several experiments are designed in the next section.

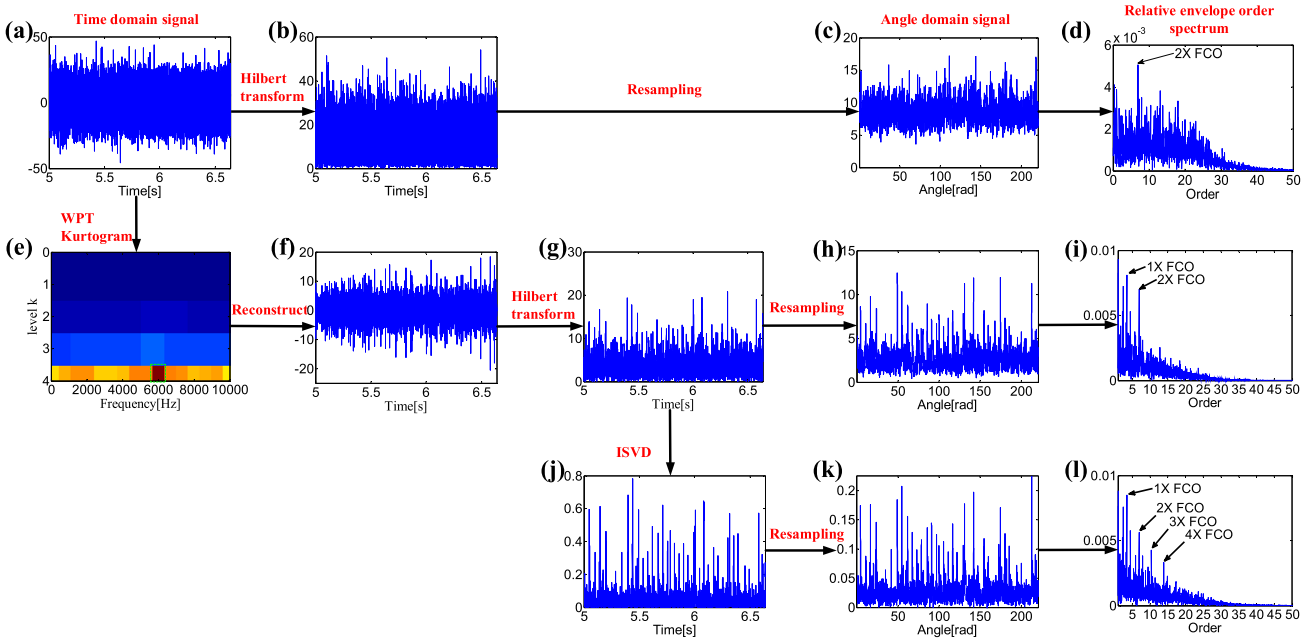

FIGURE 4. Simulated signal analysis result.

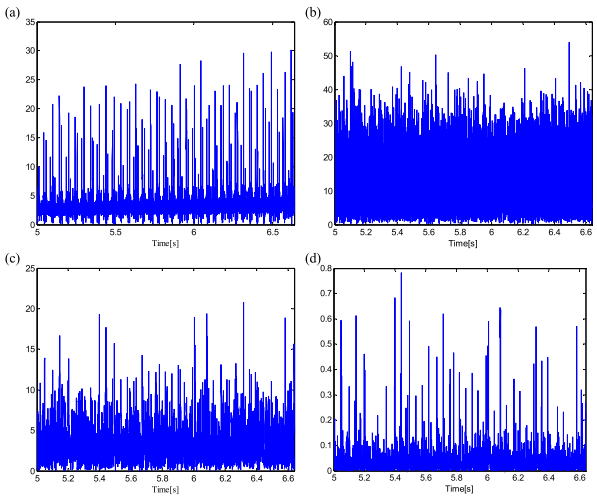

FIGURE 5. Signal envelope: (a) original signal without noise, (b) noise added signal, (c) reconstructed signal after WPTK, and (d) de-noising signal after ISVD.

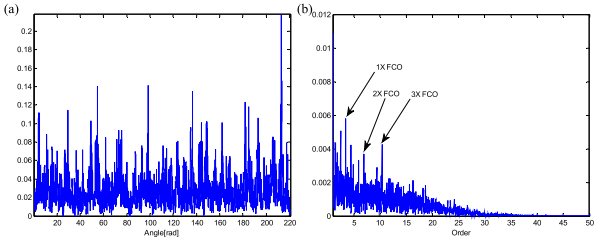

FIGURE 6. (a) The signal envelope obtained by the spectral subtraction method, (b) the relative envelope order spectra.

V. EXPERIMENTAL TESTS

To further examine the effectiveness of the proposed algorithm, an experiment is carried out on a Spectra Quest

TABLE 2. The relative amplitudes of different components.

Component	1*FCO	2*FCO	3*FCO	4*FCO
Reconstructed signal	\	0.0050	\	\
Spectral subtracted signal	0.0058	0.0037	0.0043	\
ISVD of reconstructed signal	0.0085	0.0056	0.0043	0.0033

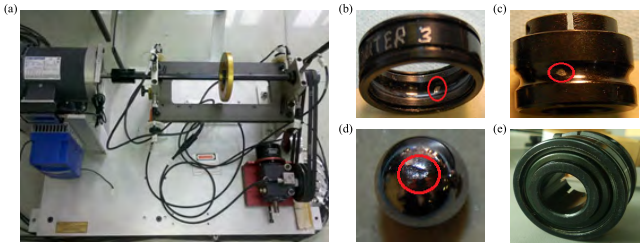

FIGURE 7. Experimental setup. (a) The bearing fault simulation bench, (b) the outer race fault, (c) the inner race fault, (d) the ball fault, and (e) the normal bearing.

Machinery Fault Simulator. The experimental setup is shown in Fig. 7 and contains a variable speed motor that is controlled by a frequency converter, a flexible coupling to connect the shaft to the motor, a tachometer mounted on the motor, a rotor disk mounted on the shaft, the outboard bearing housing, and two rolling element bearings. One of the bearings without defects is located in the bearing housing closer to the motor, and the other one is located farther from the motor. ICP acceleration sensors are fixed on the bearing housing to collect vibration signals at a sampling frequency of 20 kHz.

In this experiment, a normal bearing is installed in the inboard bearing housing, and a series of bearings are located in the outboard bearing housing to simulate the health conditions: (1) normal, (2) bearing with an inner race fault,

(3) bearing with an outer race fault, and (4) bearing with a ball fault. The bearing parameters are listed in Table 3.

TABLE 3. Parameters of the bearings.

Component	Number of balls	Contact angle	Pitch diameter	Ball diameter	BPFO	BPFI	BSF
ER-12K	8	0	1.318 in	0.3125 in	3.048	4.95	1.992

The fault characteristic orders (FCOs) are applied to monitor the health status of the bearing at time-varying speed conditions. The outer race fault characteristic order FCO_o, the inner race fault characteristic order FCO_i and the rolling element fault characteristic order FCO_b are formulated as follows:

$$FCO_o = \frac{Z}{2}\left(1 - \frac{d}{D}\cos\alpha\right) \tag{16}$$

$$FCO_i = \frac{Z}{2}\left(1 + \frac{d}{D}\cos\alpha\right) \tag{17}$$

$$FCO_b = \frac{Z}{2d}\left(1 - (\frac{d}{D})^2\cos^2\alpha\right) \tag{18}$$

where Z is the number of rolling elements, α is the contact angle, and d and D are the diameter of the rolling element and pitch diameter, respectively.

A. OUTER RACE FAULT CASE

In this experiment, the vibration signal is obtained when the shaft rotates in [22, 25] Hz. The signal and its frequency spectrum are shown in Fig. 8 (a) and (b), respectively. The speed information is shown in Fig. 8 (c).

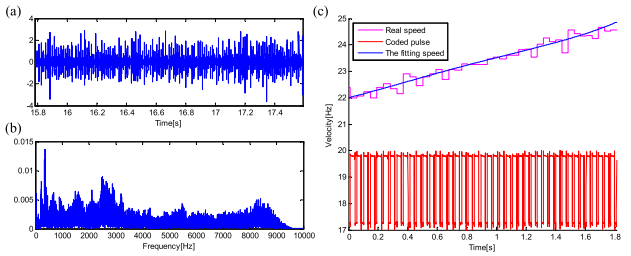

FIGURE 8. (a) The time-domain signal, (b) the frequency spectrum, and (c) the rotating speed.

The optimal frequency band of the WPT kurtogram is [8750, 9375] Hz, as shown in Fig. 9 within the green rectangle at level 4, and the corresponding coefficient of the WPT is used to reconstruct the signal. The envelope of the extracted signal is calculated by the Hilbert transform, which is shown in Fig. 10 (a). Then, a band-pass filter, whose pass band cutoff frequency is lower than the minimum of the rotating frequency and stop band cutoff frequency is larger than the carrier frequency of the envelope of the impulse response, is used to eliminate the interference of the trend terms and the noise beyond the filtered band. The filtered signal is

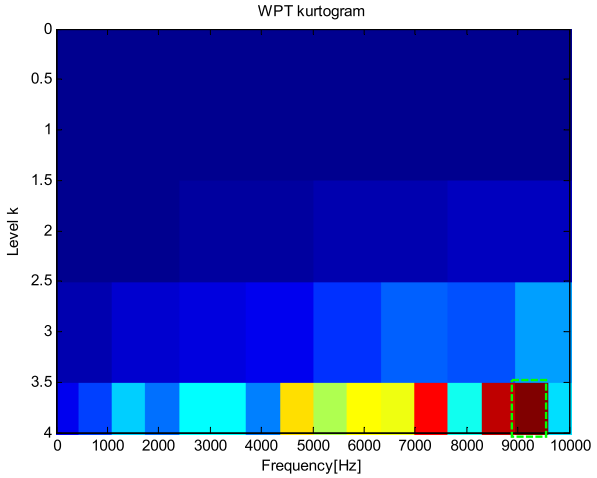

FIGURE 9. The WPT kurtogram.

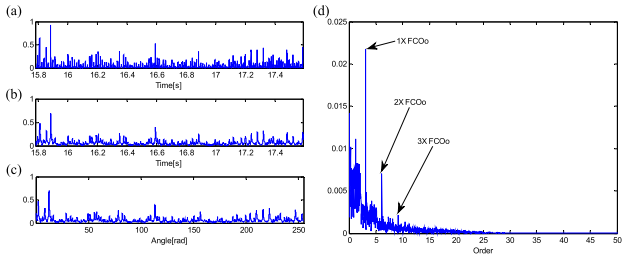

FIGURE 10. (a) The reconstructed signal envelope, (b) the filtered signal of the envelope, (c) the resampling signal of the filtered signal, and (d) the relative envelope order spectra.

shown in Fig. 10 (b). The filtered signal is resampled into the angular domain to eliminate the influence of varying speed, and an angular signal is obtained, as shown in Fig. 10 (c). The FCO domain information is obtained by using the FFT of the angular signal. For the sake of comparison, the relative amplitude of the spectrum is calculated by Eq. (14), and the spectrum is shown in Fig. 10 (d). In Fig. 10 (d), although the first two orders of the outer race fault order are clear, the third order is too small to be found due to the in-band noise influence. According to the literature [31], this method is not good for the fault type identified.

To further enhance the SNR, the envelope in Fig. 10 (a) is processed by ISVD. The prior threshold of the RMSE between the adjacent envelopes is set to 0.03, i.e., $\lambda_m = 0.03$., and the cross-correlation coefficient is set to 0.99, i.e., $\lambda_c = 0.99$. A high-pass filter, whose cutoff frequency is lower than the minimum speed value, is used to eliminate the trend terms of the envelopes in the program iteratively. When $\lambda_m < 0.03$, the iteration ends, and the signal corresponding to the maximum SK value is extracted, as shown in Fig. 11 (a). The corresponding resampling signal is shown in Fig. 11 (b). Compared with Fig. 10 (d), the amplitude of the first three orders is larger and the 4th is clearer in the relative order spectra, which is shown in Fig. 11 (c). Similar to the simulation, the spectral subtraction method is also applied to the experimental signal to validate the efficacy of the proposed method. In Fig. 12, only the first two orders of the outer race

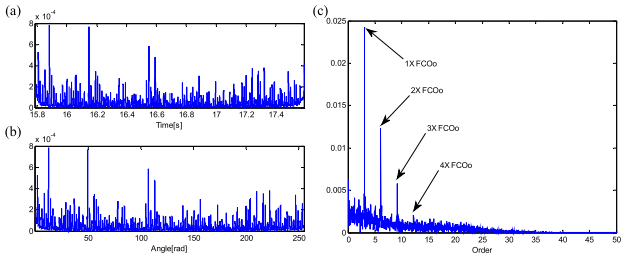

FIGURE 11. (a) The in-band de-noised envelope signal, (b) the resampling envelope signal, and (c) the relative envelope order spectra.

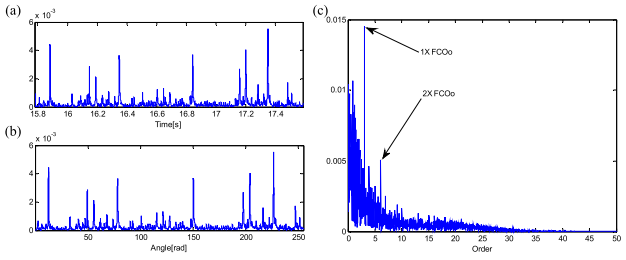

FIGURE 12. Spectral subtraction method: (a) the in-band de-noised envelope signal, (b) the resampling envelope signal, and (c) the relative order spectra.

TABLE 4. The relative amplitudes of different components.

Component	1*FCO_o	2*FCO_o	3*FCO_o	4*FCO_o
Reconstructed signal	0.0217	0.0070	0.0021	\
Spectral subtracted signal	0.0146	0.0051	\	\
ISVD of reconstructed signal	0.0242	0.0124	0.0058	0.0021

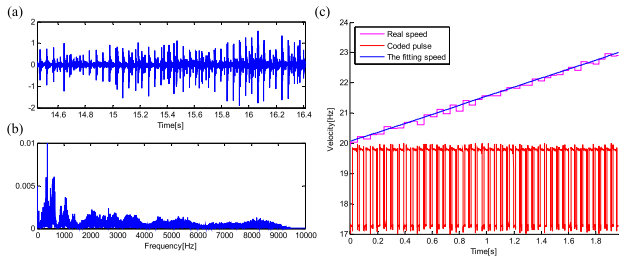

FIGURE 13. (a) The time-domain signal, (b) the frequency spectrum, and (c) the rotating speed.

fault order can be found. For convenience of comparison, the amplitudes of different components are shown in Table 4.

B. INNER RACE FAULT CASE

In this experiment, the vibration signal is collected during the shaft rotation from 20 Hz to 23 Hz, and its frequency spectrum information is shown in Fig. 13.

In Fig. 14, the optimal frequency band of the WPT kurtogram is [8125, 8750] Hz. The envelope of the extracted signal and its relative order spectrum are shown in Fig. 15 (a-d). This spectrum contains strong components related to shaft rotation harmonics, and FCO_i is 4.95, which is nearly an integer multiple of the shaft rotation

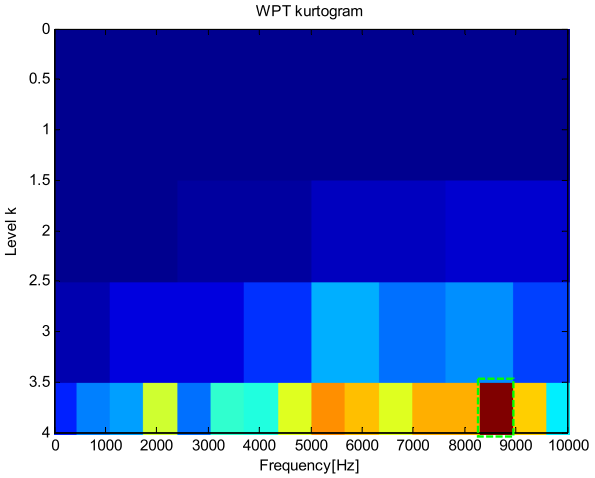

FIGURE 14. The WPT kurtogram.

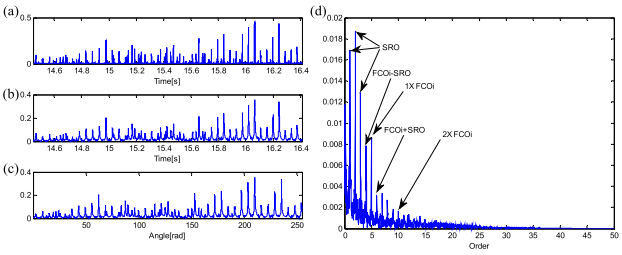

FIGURE 15. (a) The reconstructed signal envelope, (b) the filtered signal of the envelope, (c) the resampling signal of the filtered signal, and (d) the relative envelope order spectra.

order (SRO), so it is difficult to distinguish between them. In other words, although the first two orders of the inner race fault order are clear, it is not easy in recognize the defect related order information directly from the spectral map in Fig. 15(d).

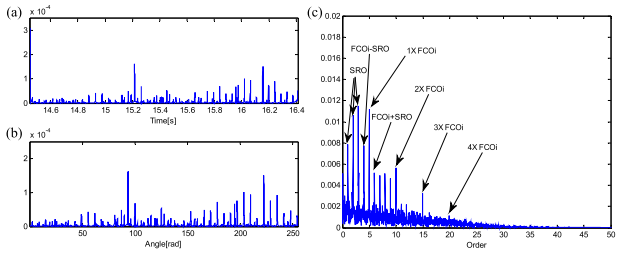

FIGURE 16. (a) The in-band de-noised envelope signal, (b) the resampling envelope signal, and (c) the relative order spectra.

The signal is processed by ISVD. In the ISVD program, the threshold of the RMSE $\lambda_m = 0.01$, the cross-correlation coefficient $\lambda_c = 0.99$, and the cutoff frequency of the high-pass filter for trend term elimination is set to 20 Hz. The analysis result is shown in Fig. 16. The relative amplitude near FCO_i is significantly larger than that of the sidebands on both sides. Moreover, the third fault characteristic order is clear. The spectral subtraction is also applied to the experimental signal. As shown in Fig. 17, the spectral subtraction method

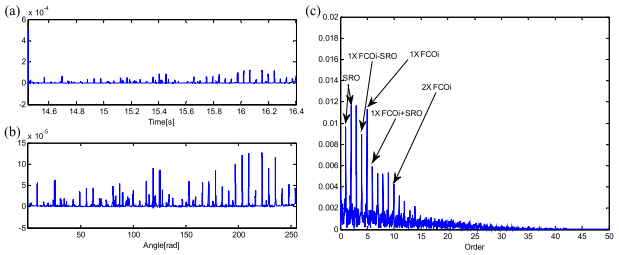

FIGURE 17. Spectral subtraction method: (a) the in-band de-noised envelope signal, (b) the resampling envelope signal, and (c) the relative order spectra.

TABLE 5. The relative amplitudes of different components.

Component	$1*FCO_i$	$2*FCO_i$	$3*FCO_i$	$4*FCO_i$
Reconstructed signal	0.0087	0.0017	\	\
Spectral subtracted signal	0.0113	0.0043	\	\
ISVD of reconstructed signal	0.0112	0.0056	0.0033	0.0012

successfully extracts the inner race fault feature. Nevertheless, only the first two orders of the inner race fault order protrude in the relative order spectra, and they are difficult to distinguish from the interference of the orders of the shaft rotation order. The amplitudes of different components are compared in Table 5.

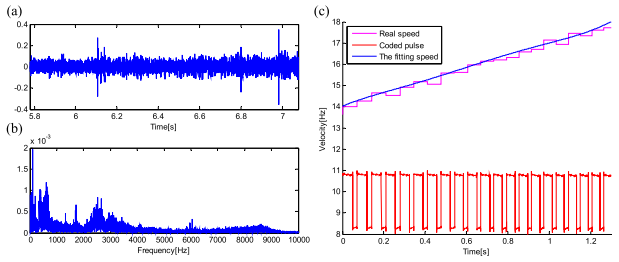

FIGURE 18. (a) The time-domain signal, (b) the frequency spectrum, and (c) the rotating speed.

C. BALL FAULT CASE

Compared with the inner and outer race fault signals, the fault impulses are not obvious in the ball fault vibration signal. In this experiment, the signals are collected when the shaft rotates from 14 Hz to 18 Hz. The time domain signal and its frequency spectrum are shown in Fig. 18 (a) and (b), respectively. The rotating speed is shown in Fig. 18 (c).

In the WPT kurtogram, the recommended frequency band is located at the 4th level during the bands of [3125, 3750] Hz, as shown in Fig. 19 within the green rectangle.

The filtered signal analysis results are shown in Fig. 20 (a-d) and Fig. 21 (a-c). Similar to the experiments mentioned above, the ISVD is used here. The prior threshold of the RMSE between the adjacent envelopes λ_m is set to 0.003 and the cross-correlation coefficient λ_c is set to 0.99. The cutoff frequency of the high-pass filter is 14 Hz. The first three orders of the ball fault order are visible in the relative order spectrum by the proposed method,

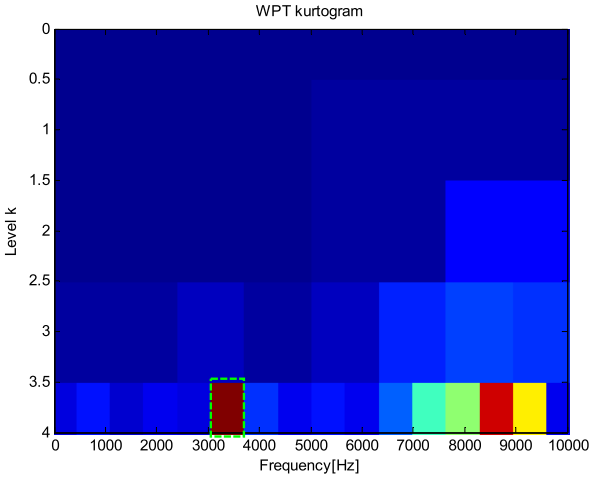

FIGURE 19. The WPT kurtogram.

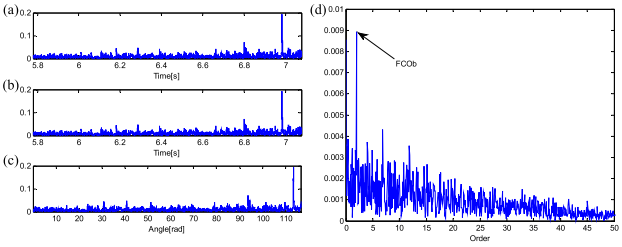

FIGURE 20. (a) The reconstructed signal envelope, (b) the filtered signal of the envelope, (c) the resampling signal of the filtered signal, and (d) the relative envelope order spectra.

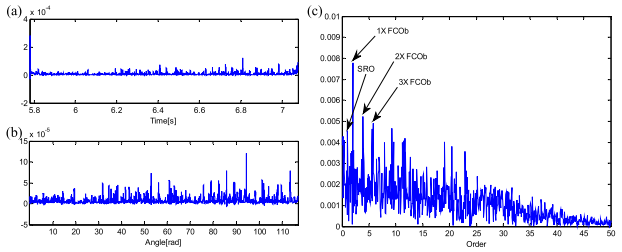

FIGURE 21. (a) The in-band de-noised envelope signal, (b) the resampling envelope signal, and (c) the relative envelope order spectra.

as shown in Fig. 21(c), while only the first order of the ball fault order can be seen in the relative order spectra shown in Fig. 20 (d).

Similar to the experiments above, the spectral subtraction method is also applied to this signal, and the results are shown in Fig. 22. However, the optimal frequency band in the WPT kurtogram does not correspond to the carrier frequency, and the envelope obtained by the spectral subtraction method includes no fault information. For convenience of comparison, the amplitudes of the different components are compared in Table 6.

D. NORMAL CASE

To demonstrate the effectiveness of the proposed method, the faulty bearing is replaced with a normal bearing using the same setup, and the analysis results are shown in Figs. 23-25.

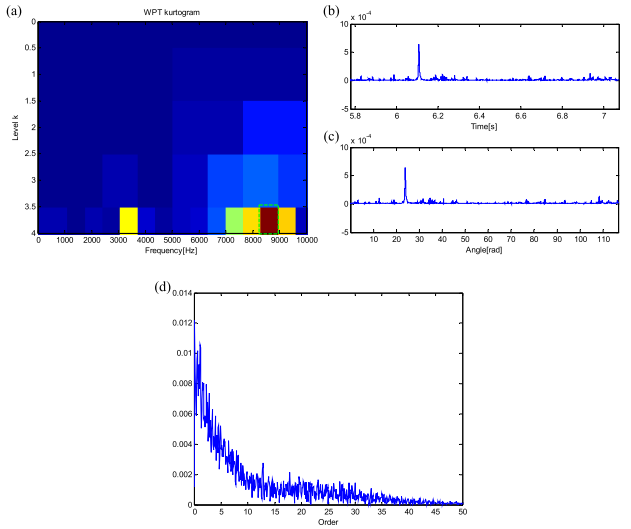

FIGURE 22. Spectral subtraction method: (a) the WPT kurtogram, (b) the in-band de-noised envelope signal, (c) the resampling envelope signal, and (d) the relative envelope order spectra.

TABLE 6. The relative amplitudes of different components.

Component	1*FCO_b	2*FCO_b	3*FCO_b
Reconstructed signal	0.0089	\	\
Spectral subtracted signal	\	\	\
ISVD of reconstructed signal	0.0078	0.0051	0.0049

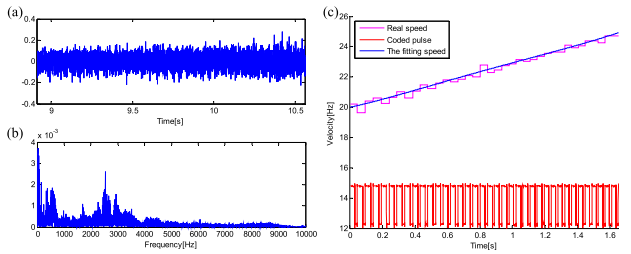

FIGURE 23. (a) The time-domain signal, (b) the frequency spectrum, and (c) the rotating speed.

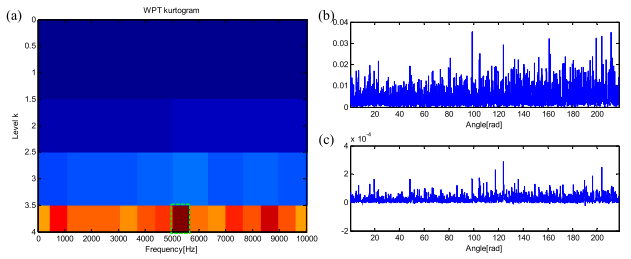

FIGURE 24. (a) The WPT kurtogram. The resampling envelope signal: (b) before the ISVD process, and (c) after the ISVD process.

The recommended frequency band of the WPT kurtogram is [5000, 5625] Hz, as shown in Fig. 24 (a). The resampling envelope signals are shown in Fig. 24 (b) and (c). Compared with Fig. 25(a), after the ISVD process, the relative amplitude of the shaft rotation order and its octaves are higher than

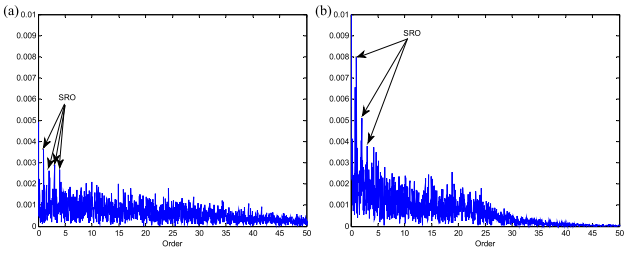

FIGURE 25. The relative order spectrum: (a) before the ISVD process and (b) after the ISVD process.

the previous one, which is shown in Fig. 25(b). This further indicates that ISVD can improve the in-band SNR effectively.

VI. CONCLUSIONS

In this study, an iterated SVD-based in-band noise reduction method combined with envelope order spectra is proposed for bearing fault diagnosis under varying speed conditions. To avoid the destruction of useful information caused by excessive iteration, a threshold is set to determine the number of iterations and correlation analysis is used to improve the computational efficiency. A de-noised signal is reconstructed based on the relationship between the singular value and a frequency component. Compared with the spectral subtraction method, although this approach may also reduce the intensity of frequency components other than the white noise, it helps the hidden impulses to manifest in the final de-noised signal, which is helpful to improve SNR. Finally, the enhanced non-stationary signal envelope is resampled and transformed into the fault characteristic order domain where the bearing fault type can be identified from the envelope order spectra. It is worth mentioning that the threshold of iterations has great influence on the fault diagnosis results, which is caused by the defects of SVD itself, and excessive iterative decomposition will destroy the useful information of the original signal. Besides, the envelope spectrum kurtosis index will fail to locate the sensitive frequency band when the noise components is strong enough. Therefore, our work will focus on solving the above problems in the future.

APPENDIX

A Hankel matrix $H_{m\times n}$, the rank of it is $rank(H_{m\times n}) \leq min(m, n)$, while the number of non-zero singular values of the matrix is equal to the rank, i.e. $\sigma_{numb} = rank(H_{m\times n})$. Taking the case that $n \geq m$ as an example to explain the relationship between the signal length and the number of frequency components included that should be satisfied, the same as $m > n$.

$$\begin{cases} f_{numb} = \sigma_{numb}/2 \\ \sigma_{numb} = 2k, k = 1, 2, \cdots, floor(m/2) \\ f_{numb} = \sigma_{numb} \pm 1/2 \\ \sigma_{numb} = 2k \pm 1, k = 1, 2, \cdots, floor(m/2) \end{cases} \tag{19}$$

Therefore,

$$rank(H_{m\times n}) = \sigma_{numb} = (2 \times f_{numb}) \pm (0, 1) \leq m.$$

So,

$$\begin{cases} N = m + n - 1 \\ m = N + 1 - n \\ N + 1 - n \geq (2 \times f_{numb}) \pm (0, 1) \\ N \geq (2 \times f_{numb}) \pm (0, 1) + n - 1 \\ \geq (2 \times f_{numb}) \pm (0, 1) + m - 1 \\ \geq 2 \times [(2 \times f_{numb}) \pm (0, 1)] - 1 \\ = (4 \times f_{numb}) \pm (0, 2) - 1 \end{cases}$$

REFERENCES

[1] D. Zhao, J. Li, W. Cheng, and W. Wen, "Compound faults detection of rolling element bearing based on the generalized demodulation algorithm under time-varying rotational speed," *J. Sound Vibrat.*, vol. 378, pp. 109–123, Sep. 2016.
[2] C. Mishra, A. K. Samantaray, and G. Chakraborty, "Rolling element bearing defect diagnosis under variable speed operation through angle synchronous averaging of wavelet de-noised estimate," *Mech. Syst. Signal Process.*, vols. 72–73, pp. 206–222, May 2016.
[3] S. Zhang, S. Lu, Q. He, and F. Konga, "Time-varying singular value decomposition for periodic transient identification in bearing fault diagnosis," *J. Sound Vibrat.*, vol. 379, pp. 213–231, Sep. 2016.
[4] Z. Li, Y. Jiang, C. Hu, and Z. Peng, "Difference equation based empirical mode decomposition with application to separation enhancement of multi-fault vibration signals," *J. Difference Equ. Appl.*, vol. 23, nos. 1–2, pp. 457–467, Feb. 2017.
[5] Y. Ren, W. Li, Z. Zhu, Z. Tong, and G. Zhou, "A new fault feature for rolling bearing fault diagnosis under varying speed conditions," *Adv. Mech. Eng.*, vol. 9, no. 6, pp. 1–11, 2017.
[6] D. Wang, K.-L. Tsui, "Dynamic Bayesian wavelet transform: New methodology for extraction of repetitive transients," *Mech. Syst. Signal Process.*, vol. 88, pp. 137–144, May 2017.
[7] T. Wang, F. Chu, Q. Han, and Y. Kong, "Compound faults detection in gearbox via meshing resonance and spectral kurtosis methods," *J. Sound Vibrat.*, vol. 392, pp. 367–381, Mar. 2017.
[8] D. Wang, P. W. Tse, and K. L. Tsui, "An enhanced Kurtogram method for fault diagnosis of rolling element bearings," *Mech. Syst. Signal Process.*, vol. 35, nos. 1–2, pp. 176–199, Feb. 2013.
[9] P. D. Mcfadden and J. D. Smith, "Vibration monitoring of rolling element bearings by the high-frequency resonance technique—A review," *Tribol. Int.*, vol. 17, no. 1, pp. 3–10, 1984.
[10] I. S. Bozchalooi and M. Liang, "Identification of the high SNR frequency band for bearing fault signature enhancement," in *Proc. 14th Int. Conf. Mechatron. Mach. Vis. Pract.*, Dec. 2007, pp. 39–43.
[11] R. Dwyer, "Detection of non-Gaussian signals by frequency domain Kurtosis estimation," in *Proc. IEEE Int. Conf. Acoust., Speech, Signal Process.* Apr. 1983, pp. 607–610.
[12] J. Antoni, "Fast computation of the Kurtogram for the detection of transient faults," *Mech. Syst. Signal Process.*, vol. 21, no. 1, pp. 108–124, 2007.
[13] X. Chen, F. Feng, and B. Zhang, "Weak fault feature extraction of rolling bearings based on an improved Kurtogram," *Sensors*, vol. 16, no. 9, p. 1482, 2016.
[14] Y. Lei, J. Lin, Z. He, and Y. Zi, "Application of an improved Kurtogram method for fault diagnosis of rolling element bearings," *Mech. Syst. Signal Process.*, vol. 25, no. 5, pp. 1738–1749, 2011.
[15] I. S. Bozchalooi and M. Liang, "A joint resonance frequency estimation and in-band noise reduction method for enhancing the detectability of bearing fault signals," *Mech. Syst. Signal Process.*, vol. 22, no. 4, pp. 915–933, 2008.
[16] M. Zhao, J. Lin, Y. Miao, and X. Xu, "Detection and recovery of fault impulses via improved harmonic product spectrum and its application in defect size estimation of train bearings," *Measurement*, vol. 91, pp. 421–439, Sep. 2016.
[17] W. Wang, and H. Lee, "An energy kurtosis demodulation technique for signal denoising and bearing fault detection," *Meas. Sci. Technol.*, vol. 24, no. 2, 2013, Art. no. 025601.
[18] M. Zhao and X. Jia, "A novel strategy for signal denoising using reweighted SVD and its applications to weak fault feature enhancement of rotating machinery," *Mech. Syst. Signal Process.*, vol. 94, pp. 129–147, Sep. 2017.
[19] R. Golafshan and K. Y. Sanliturk, "SVD and Hankel matrix based denoising approach for ball bearing fault detection and its assessment using artificial faults," *Mech. Syst. Signal Process.*, vols. 70–71, pp. 36–50, Mar. 2016.
[20] X. Zhao and B. Ye, "Singular value decomposition packet and its application to extraction of weak fault feature," *Mech. Syst. Signal Process.*, vols. 70–71, pp. 73–86, Mar. 2016.
[21] A. BÃűttcher and S. M. Grudsky, "Toeplitz matrices, asymptotic linear algebra and functional analysis," in *Toeplitz Matrices, Asymptotic Linear Algebra, and Functional Analysis*. Basel, Switzerland: Birkhäuser, 2000, p. 312.
[22] A. Zhang, "The property of cycle matrix and cycle matrix diagonalization," *J. Guangxi Teachers College*, vol. 17, no. 4, pp. 10–13, Dec. 2000.
[23] P. Jain and R. B. Pachori, "Event-based method for instantaneous fundamental frequency estimation from voiced speech based on eigenvalue decomposition of the Hankel matrix," *IEEE/ACM Trans. Audio, Speech, Language Process.*, vol. 22, no. 10, pp. 1467–1482, Oct. 2014.
[24] Z. Qiao and Z. Pan, "SVD principle analysis and fault diagnosis for bearings based on the correlation coefficient," *Meas. Sci. Technol.*, vol. 26, no. 8, 2015, Art. no. 085014.
[25] Z. Li, Y. Jiang, Q. Guo, C. Hu, and Z. Peng, "Multi-dimensional variational mode decomposition for bearing-crack detection in wind turbines with large driving-speed variations," *Renew. Energy*, vol. 116, pp. 55–73, Feb. 2018.
[26] S. Lu, X. Wang, Q. He, F. Liu, and Y. Liu, "Fault diagnosis of motor bearing with speed fluctuation via angular resampling of transient sound signals," *J. Sound Vibrat.*, vol. 385, pp. 16–32, Dec. 2016.
[27] Z. Wu and N. E. Huang, "A study of the characteristics of white noise using the empirical mode decomposition method," *Proc. Math. Phys. Eng. Sci.*, vol. 460, no. 2046, pp. 1597–1611, Jun. 2004.
[28] A. B. Ming, W. Zhang, Z. Y. Qin, and F. L. Chu, "Fault feature extraction and enhancement of rolling element bearing in varying speed condition," *Mech. Syst. Signal Process.*, vols. 76–77, pp. 367–379, Aug. 2016.
[29] Y. Wang, J. Xiang, R. Markert, and M. Liang, "Spectral kurtosis for fault detection, diagnosis and prognostics of rotating machines: A review with applications," *Mech. Syst. Signal Process.*, vol. 66–67, pp. 679–698, 2016.
[30] D. Bianchi, E. Mayrhofer, M. Gröschl, G. Betz, and A. Vernes, "Wavelet packet transform for detection of single events in acoustic emission signals," *Mech. Syst. Signal Process.*, vols. 64–65, pp. 441–451, Dec. 2015.
[31] X. Gu, S. Yang, Y. Liu, and R. Hao, "Rolling element bearing faults diagnosis based on Kurtogram and frequency domain correlated kurtosis," *Meas. Sci. Technol.*, vol. 27, no. 12, Nov. 2016, Art. no. 125019.
[32] F. Hou, J. Chen, and G. Dong, "Weak fault feature extraction of rolling bearings based on globally optimized sparse coding and approximate SVD," *Mech. Syst. Signal Process.*, vol. 111, pp. 234–250, Oct. 2018.
[33] D. Ho and R. B. Randall, "Optimisation of bearing diagnostic techniques using simulated and actual bearing fault signals," *Mech. Syst. Signal Process.*, vol. 14, no. 5, pp. 763–788, Sep. 2000.

Authors' photographs and biographies not available at the time of publication.